Hindawi Publishing Corporation
Journal of Nanomaterials
Volume 2013, Article ID 917948, 7 pages
http://dx.doi.org/10.1155/2013/917948

Research Article

Photocatalytic and Magnetic Behaviors Observed in $BiFeO_3$ Nanofibers by Electrospinning

Xuehui Zhang,[1] Haiyang Liu,[1] Bin Zheng,[2] Yuanhua Lin,[1] Deping Liu,[3] and Ce-Wen Nan[1]

[1] *State Key Laboratory of New Ceramics and Fine Processing, Department of Materials Science and Engineering, Tsinghua University, Beijing 100084, China*
[2] *Department of Materials Science and Engineering, Beijing University of Chemical Technology, Beijing 100029, China*
[3] *Department of Cardiology, Beijing Hospital, The Ministry of Health, Beijing 100730, China*

Correspondence should be addressed to Yuanhua Lin; linyh@tsinghua.edu.cn

Received 4 May 2013; Accepted 31 May 2013

Academic Editor: Jiamin Wu

Perovskite-type $BiFeO_3$ nanofibers with wave nodes-like morphology were prepared by electrospinning. The nanofibers show a highly enhanced visible-light-active photocatalytic property. The results also showed that the diameter could affect the band gap and photocatalytic performances of nanofibers. Additionally, weak ferromagnetic behaviors can be observed at room temperature, which should be correlated to the size-confinement effect on the magnetic ordering of $BiFeO_3$ structure.

1. Introduction

$BiFeO_3$ (BFO), as a kind of multiferroic materials, which shows simultaneously spontaneous magnetic and electric ordering, has attracted much attention [1–3]. According to recent studies, BFO is also an important visible-light responsive semiconductor photocatalyst for water splitting and degradation of organic pollutants due to its suitable band gap (~2.2 eV) and excellent chemical stability [4, 5]. The synthesis method used to obtain the desired nanostructures plays a crucial role in affecting electric, magnetic, and optical properties of nanoscale BFO. Various procedures have been developed to synthesize BFO nanostructure materials such as nanoparticles [6–9], nanocubes [10, 11], nanotubes [12, 13], and nanowires [14, 15]. Gao and his coworkers reported the synthesis of BFO nanoparticles by a sol-gel technique and their photocatalytic and magnetic properties [6]. Joshi et al. investigated a microwave synthesis of single crystalline perovskite BFO nanocubes [10]. Templates methods were used to prepare BFO nanotubes [12] and nanowires [15], respectively, but there were some disadvantages including low-yield, polycrystalline structure and easy agglomeration.

Electrospinning as a simple and effective method for fabricating ultrathin nanofibers has been used widely [16–18]. Xie et al. prepared BFO nanofibers of the polycrystalline structure fired under a protective atmosphere [19]. In addition, there were some researchers investigated the ferroelectricity [20, 21] and photocatalytic activity under UV-light irradiation [22, 23] in electrospun BFO nanofibers. However, to our knowledge, there are no reports that focused on the BFO nanofibers as a visible-light-active photocatalytic decomposition material. In the present work, we reported the successful synthesis of BFO ultralong nanofibers by electrospinning and investigated the photocatalytic activity under visible light and their magnetic behaviors.

2. Materials and Methods

BFO ultrafine fibers were synthesized by electrospinning as follows. The $BiFeO_3$ precursor was prepared as previously reported [24]. The precursor was prepared from citrate acid-based solution, using iron (III) nitrate nonahydrate (99.99%, Alfa Aesar), bismuth (III) nitrate pentahydrate with a purity of 98% (Alfa Aesar), citrate acid (Sigma Aldrich) as the solutes, and N,N-dimethylformamide (DMF, China National Chemicals Corporation Ltd.) as the solution. The final concentration of the two precursor solutions were 0.2 M and 0.4 M, respectively. Excess Bi of about 5 mol% was used to

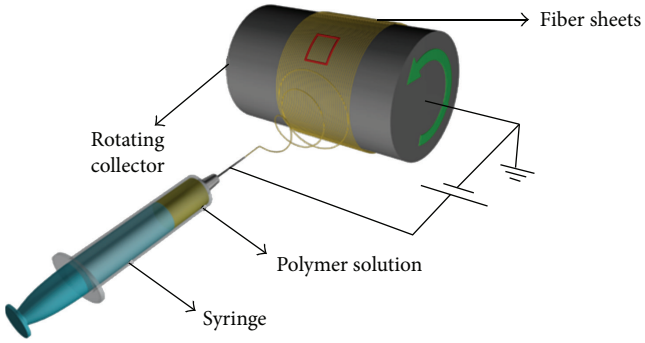

Figure 1: Schematic illustration for preparation of nanofibers by electrospinning.

compensate for the bismuth loss during the heating process. Polyvinylpyrrolidone (PVP, Mw=1,300,000 g/mol, Aldrich) was then added to the solution directly and stirred for 6 h at room temperature to obtain homogeneous solution for the electrospinning process.

This solution was fed into 20 mL syringe and electrospun through 0.5 mm diameter needle using an electrostatic spinning apparatus (Figure 1). The flow rate of spinning solution was maintained to 0.5 mL/h using a syringe pump, and an applied voltage was kept at 15 kV. The as-spun nanofibrous membranes were collected on an aluminium roller with a diameter of 100 mm at a rotating speed of 1000 rpm. The distance between the needle tip and the roller was 15 cm. And then the as-spun nanofibrous membranes were stabilized at 150°C for 10 min in air and heated at 600°C for 2 h in air to obtain the BFO nanofibers. The heating rate was kept at 10°C/min.

The crystallinity and morphology of the BFO nanofibers were examined by X-ray diffraction (XRD, Rigaku D/max 2500 V, Rigaku Corporation), scanning electron microscopy (SEM, JSM-7001F, JEOL Ltd.), and high-resolution TEM (HRTEM, JEOL2011). The average diameters of the nanofibers were calculated from 100 filaments based on the SEM images using image analysis software (Image J, National Institutes of Health, USA). The Raman spectrum measurements were performed in backscattering geometry with a radiation of Ar^+ laser at 633 nm by using a microscope-based Raman spectroscopy system (LabRAM HR, Horiba, NJ, USA). UV-visible diffuse reflectance absorption spectra were measured by a UV-vis spectrophotometer (Hitachi UV-3310). The magnetization of the samples was measured using superconducting quantum interference device (SQUID, MPMS-7, Quantum Design, San Diego, CA, USA) magnetometer. The photocatalytic activities were evaluated by the degradation of Congo red (CR) in aqueous solution under visible-light irradiation using a 500 W Xe lamp with a cutoff filter ($\lambda >$ 400 nm) according to our previous study [25]. Briefly, aqueous suspensions of CR (50 mL, 20 mg/L) and BFO nanofibers (2 g/L) were placed in an open reactor, and the suspension was placed in darkness for one hour with magnetic stirring before irradiation to reach absorption/desorption equilibrium. The reaction temperature was kept at room temperature by cooling water to prevent any thermal catalytic effect. The degradation of CR was evaluated by centrifuging the retrieved samples and recording the intensity of absorption peak of CR (495 nm) relative to its initial intensity (C/C_0) using a spectrophotometer.

3. Results and Discussion

Figure 2 shows SEM images of as-spun BFO-gel/PVP fibers and BFO nanofibers. The as-spun fibers (Figures 2(a) and 2(c)) are round in shape and have a rather uniform diameter over its length. The average diameter increased from 300 nm to 800 nm as the concentration of the solution increased from 0.2 M to 0.4 M. Figures 2(b) and 2(d) show that the BFO nanofibers have a reduced diameter of 100 nm and 300 nm after being heated. The reduction in diameter can be attributed to the thermal treatment, which has pyrolyzed the polymer at 600°C. In addition, the fibers surface became rougher after heating and annealing, which could be mainly assigned to a dramatic change in crystal structure [22].

The XRD patterns of the BFO nanofibers are shown in Figure 3(a). The reflection peaks of the different samples can be indexed as a single-phase perovskite structure belonging to the space group R3c (JCPDS card no. 86-1518), and no obvious peaks from other phase were detected, demonstrating that well-crystallized single phase BFO can be obtained under the current synthesis conditions. Fe_3O_4 and γ-Fe_2O_3 are not present as impurity phases according to the XRD pattern recorded at a very slow scan rate in the regions (33°–36° and 48°–50°) where the maximum intense peaks of γ-Fe_2O_3 and Fe_3O_4 are expected.

To get further insight on the structural variations of BFO nanofibers, typical Raman spectra of our BFO nanofibers were shown in Figure 3(b). The peaks at 140, 171, and 219 cm^{-1} can be assigned to A_1 (1TO), A_1 (2TO), and A_1 (3TO) modes for the rhombohedral BFO system, respectively, which is in good agreement with that of previously reported data [26]. Meanwhile, the E (TO) phonon modes were also quite consistent with our previous study [27].

The crystalline structure of BFO ultrafine nanofibers is further examined by HRTEM, as shown in Figure 4. It is observed from TEM images (Figures 4(a) and 4(b)) that BFO nanofibers are wave nodes-like, and the difference of diameter of nanofibers from 0.2 M and 0.4 M BFO solution was significant. The reason for this variation can rely on the increase of the concentration of the precursor solution, which results in increase of nanofibers under the same condition of electrospinning technique [28]. It indicated that the wave nodes-like morphology of nanofibers was produced by regulating the concentration of the precursor solution to a certain extent. The selected area electron diffraction (SAED) pattern from the pane area marked with dashed line in Figure 4(a) shows very sharp diffraction spots, proving the well-developed single-crystalline structure. Figure 4(c) is a HRTEM image of the grain boundary. The regular spacings of the observed lattice are 0.396 and 0.287 nm, which are corresponding to the (012) and (110) crystal planes of a rhombohedral BFO phase, respectively. This result was consistent with previous study [29].

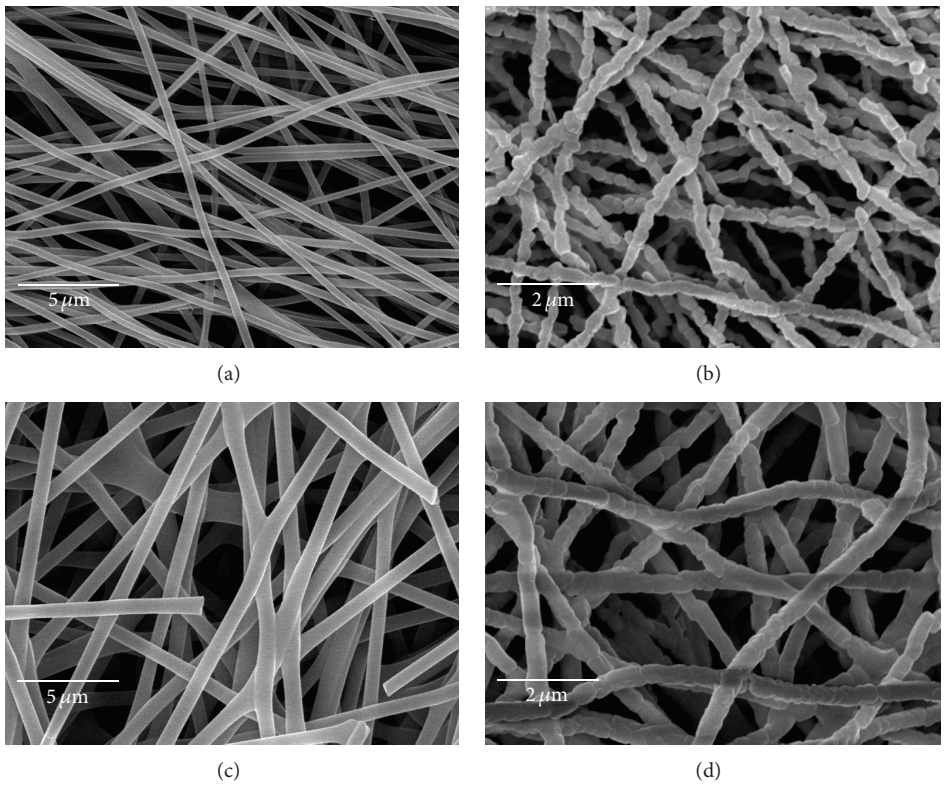

Figure 2: SEM images of (a) as-spun BFO-gel/PVP fibers without heat treatment and (b) BFO nanofibers after heat treatment synthesized with 0.2 M BFO solution; (c) as-spun BFO-gel/PVP fibers without heat treatment and (d) BFO nanofibers after heat treatment synthesized with 0.4 M BFO solution.

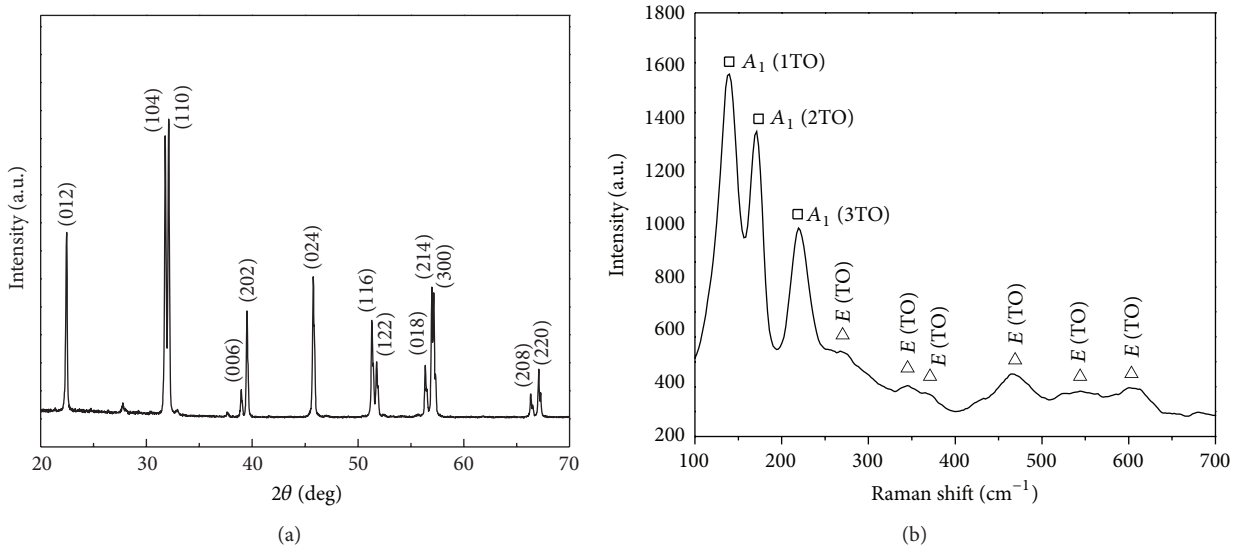

Figure 3: (a) XRD patterns of BFO nanofibers; (b) Raman spectra of BFO nanofibers.

Generally, the optical absorption performance of semiconductors is related to the electronic structure feature and their band gaps [30]. The optical properties of samples were studied by measuring their UV-vis diffuse reflectance absorption spectra. As shown in Figure 5(a), the absorption spectra of BFO nanofibers with different diameters were measured. The absorption spectra show that BFO nanofibers can absorb considerable amounts of visible light, suggesting their potential applications as visible-light-driven photocatalysts. And compared with the BFO nanofibers with the diameter of 300 nm, the BFO nanofibers with the smaller diameter (100 nm) show higher visible-light absorption. This difference was mainly due to the nanoscale size effect including ultrafine diameter and large specific surface area [31].

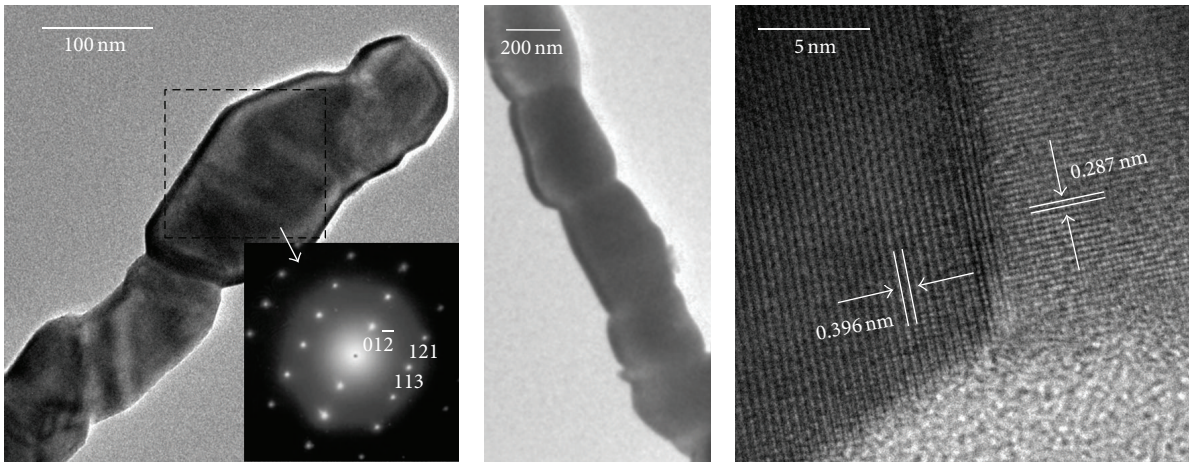

FIGURE 4: (a) TEM image of part of a single BFO nanofiber synthesized with 0.2 M BFO solution; inset is the selected area electron diffraction (SAED) pattern from the pane area marked with dashed line; (b) TEM image of part of a single BFO nanofiber synthesized with 0.4 M BFO solution; (c) HRTEM image of the grain boundary of BFO nanofibers.

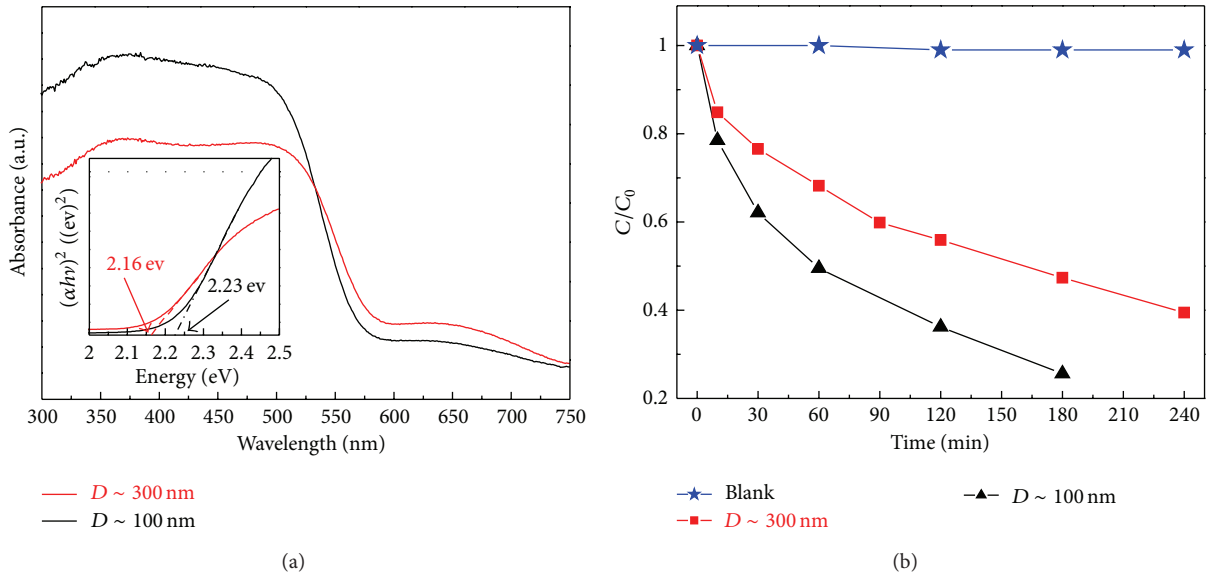

FIGURE 5: (a) UV-vis diffuse reflectance absorption spectra of BFO nanofibers with different diameters; inset is the calculation diagrams of the corresponding band gap; (b) photodegradation of CR in the presence of BFO nanofibers with different diameters under visible-light irradiation.

The optical absorption coefficient near the band edge follows [32]:

$$\alpha h\nu = A\left(h\nu - E_g\right)^{n/2}, \quad (1)$$

where α, h, ν, E_g, and A are absorption coefficient, Planck constant, light frequency, band gap, and a constant, respectively. Considering that BFO is a direct band gap material, the value of n for $BiFeO_3$ is 1 [33]. The corresponding values of direct band gap of BFO nanofibers can be evaluated by extrapolating the linear portion of $(\alpha h\nu)^2$ versus $(h\nu)$, as shown in the inset of Figure 5(a). After calculations, the values of the nanofibers with the diameters of 300 nm and 100 nm are 2.16 eV and 2.23 eV, respectively, which is quite consistent with previous results [15, 34]. The obvious shift in absorption edge for the samples may be due to the change of fibers size [35]. In addition, a secondary edge that can also be assigned to crystal field transition was observed at higher wavelengths for the nanofibers.

To further evaluate the visible light photocatalytic activity of as-synthesized samples, Congo red (CR) with a major absorption peak at 495 nm was chosen as a model organic pollutant. Visible-light irradiation of aqueous CR/BFO led to an apparent decrease in absorption. Figure 5(b) gives the concentration changes of CR at 495 nm by BFO nanofibers as a function of irradiation time under visible light during the degradation process. A dark experiment (without irradiation)

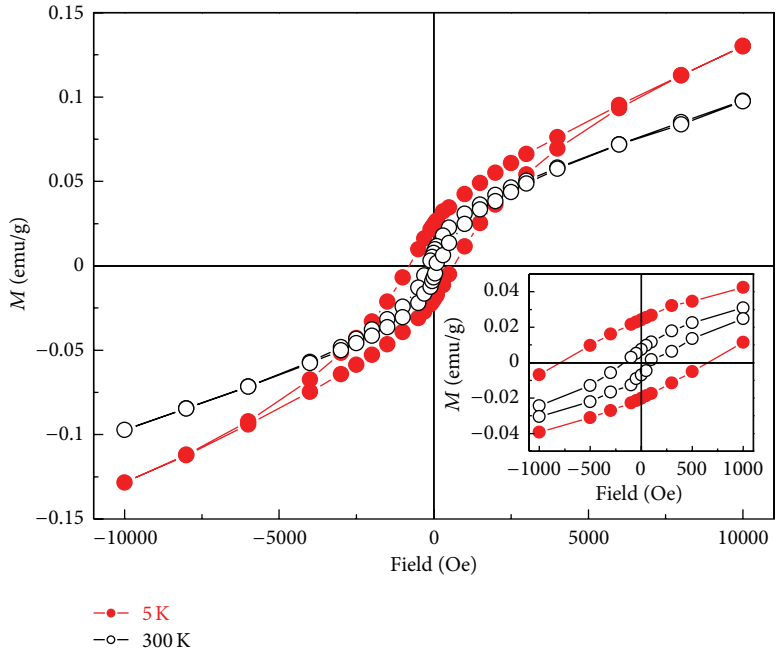

Figure 6: The magnetization hysteresis loops of BFO nanofibers at RT and 5 K, and inset is the partially enlarged curves, respectively.

was also performed, in which the CR decomposition was negligible. The BFO nanofibers show good photocatalytic efficiency. After being exposed to visible light for 3 hours, 75% of the CR was photodegraded with the BFO nanofibers of 100 nm diameter as photocatalysts, showing better photocatalytic activity than that of 300 nm diameter (50%). The reason may be that the smaller nanofibers have higher surface-area-to-volume ratios. In our earlier studies, the BFO nanoparticles with 100 nm size could only degrade almost 40% of the initial dye after 2 h under the same conditions [7], while the BFO nanofibers with the same size can degrade 65%. This can be attributed to the ultralong longitudinal dimension of nanofibers that provides a sufficiently spacious transport channel for charge separation [36]. It indicated that electrospinning technology for fabricating BFO nanofibers has more significant advantages in photocatalytic performance than other fabrication methods.

Considering the importance of the multiferroic property of BFO [37, 38], the magnetic ordering of the BFO nanofibers of 100 nm diameter was measured by SQUID (Figure 6). It is important to note that the saturated M is ~0.01 emu/g at RT, much smaller than that (~0.04 emu/g) of BFO nanowires [15] with 50 nm diameter prepared by AAO templates. It may be due to the size effect. The partially enlarged M-H curve is shown in the inset, which reveals that the RT coercive field of the BFO nanofibers is quite small (~150 Oe), similar to that of the nanoparticles [6, 8] and the nanowires [15]. The grain size of our nanofibers is larger than the 62 nm wavelength of the intrinsic spiral-modulated spin structure in bulk $BiFeO_3$ as previously reported [39]. It was reported that the cycloid structure becomes more anharmonic at lower T, and its detrimental effect on the magnetic ordering is devalued [39], leading to stronger ferromagnetics (FM), evidenced by the M-H loop at $T = 5$ K, as shown in Figure 6. These results indicated that BFO nanofibers show weak ferromagnetic at RT and 5 K, similar to that of nanoparticles.

4. Conclusions

In summary, we have successfully prepared BFO nanofibers with 100 nm and 300 nm diameters by electrospinning. These nanofibers with bamboo-like morphology show a highly enhanced visible-light-active photocatalytic property, compared with the BFO nanoparticles. Our results also showed that the diameter could affect the band gap and photocatalytic performances of nanofibers. In addition, magnetic studies revealed their weak ferromagnetic behaviors at RT and 5 K. These BFO nanofibers can be useful for developing multifunctional devices combining magnetic, electronic, and optical properties.

Acknowledgments

This work was supported by the Ministry of Science and Technology of China through a 973-Project under Grant no. 2009CB623303, NSF of China (51025205, 51272181, and 51272121).

References

[1] M. Fiebig, T. Lottermoser, D. Fröhlich, A. V. Goltsev, and R. V. Pisarev, "Observation of coupled magnetic and electric domains," *Nature*, vol. 419, no. 6909, pp. 818–820, 2002.

[2] J. Wang, J. B. Neaton, H. Zheng et al., "Epitaxial $BiFeO_3$ multiferroic thin film heterostructures," *Science*, vol. 299, no. 5613, pp. 1719–1722, 2003.

[3] S. Y. Yang, J. Seidel, S. J. Byrnes et al., "Above-bandgap voltages from ferroelectric photovoltaic devices," *Nature Nanotechnology*, vol. 5, no. 2, pp. 143–147, 2010.

[4] A. Fujishima and K. Honda, "Electrochemical photolysis of water at a semiconductor electrode," *Nature*, vol. 238, no. 5358, pp. 37–38, 1972.

[5] F. Gao, Y. Yuan, K. F. Wang et al., "Preparation and photoabsorption characterization $BiFeO_3$ nanowires," *Applied Physics Letters*, vol. 89, no. 10, Article ID 102506, pp. 2506–2508, 2006.

[6] F. Gao, X. Chen, K. Yin et al., "Visible-light photocatalytic properties of weak magnetic $BiFeO_3$ nanoparticles," *Advanced Materials*, vol. 19, no. 19, pp. 2889–2892, 2007.

[7] S. Li, Y. Lin, B. Zhang, C. Nan, and Y. Wang, "Photocatalytic and magnetic behaviors observed in nanostructured $BiFeO_3$ particles," *Journal of Applied Physics*, vol. 105, no. 5, Article ID 056105, 2009.

[8] S. Li, Y. Lin, B. Zhang, Y. Wang, and C. Nan, "Controlled fabrication of $BiFeO_3$ uniform microcrystals and their magnetic and photocatalytic behaviors," *Journal of Physical Chemistry C*, vol. 114, no. 7, pp. 2903–2908, 2010.

[9] Y. G. Wang, G. Xu, Z. H. Ren et al., "Mineralizer-assisted hydrothermal synthesis and characterization of $BiFeO_3$ nanoparticles," *Journal of the American Ceramic Society*, vol. 90, no. 8, pp. 2615–2617, 2007.

[10] U. A. Joshi, J. S. Jang, P. H. Borse, and J. S. Lee, "Microwave synthesis of single-crystalline perovskite $BiFeO_3$ nanocubes for photoelectrode and photocatalytic applications," *Applied Physics Letters*, vol. 92, no. 24, Article ID 242106, 2008.

[11] J. Chen, X. R. Xing, A. Watson et al., "Rapid synthesis of multiferroic $BiFeO_3$ single-crystalline nanostructures," *Chemistry of Materials*, vol. 19, no. 15, pp. 3598–3600, 2007.

[12] J. Wei, D. S. Xue, and Y. Xu, "Photoabsorption characterization and magnetic property of multiferroic $BiFeO_3$ nanotubes synthesized by a facile sol-gel template process," *Scripta Materialia*, vol. 58, no. 1, pp. 45–48, 2008.

[13] X. Y. Zhang, C. W. Lai, X. Zhao, D. Y. Wang, and J. Y. Dai, "Synthesis and ferroelectric properties of multiferroic $BiFeO_3$ nanotube arrays," *Applied Physics Letters*, vol. 87, no. 14, Article ID 143102, pp. 1–3, 2005.

[14] X. Y. Zhang, J. Y. Dai, and C. W. Lai, "Synthesis and characterization of highly ordered $BiFeO_3$ multiferroic nanowire arrays," *Progress in Solid State Chemistry*, vol. 33, no. 2–4, pp. 147–151, 2005.

[15] F. Gao, Y. Yuan, K. F. Wang et al., "Preparation and photoabsorption characterization $BiFeO_3$ nanowires," *Applied Physics Letters*, vol. 89, no. 10, Article ID 102506, 2006.

[16] E. Zussman, A. Theron, and A. L. Yarin, "Formation of nanofiber crossbars in electrospinning," *Applied Physics Letters*, vol. 82, no. 6, pp. 973–975, 2003.

[17] Y. Dzenis, "Spinning continuous fibers for nanotechnology," *Science*, vol. 304, no. 5679, pp. 1917–1919, 2004.

[18] D. Li and Y. Xia, "Electrospinning of nanofibers: reinventing the wheel?" *Advanced Materials*, vol. 16, no. 14, pp. 1151–1170, 2004.

[19] S. H. Xie, J. Y. Li, R. Proksch et al., "Nanocrystalline multiferroic $BiFeO_3$ ultrafine fibers by sol-gel based electrospinning," *Applied Physics Letters*, vol. 93, no. 22, Article ID 222904, 2008.

[20] A. Baji, Y. Mai, Q. Li, S. Wong, Y. Liu, and Q. W. Yao, "One-dimensional multiferroic bismuth ferrite fibers obtained by electrospinning techniques," *Nanotechnology*, vol. 22, no. 23, Article ID 235702, 2011.

[21] J. H. Song, J. H. Nam, J. H. Cho, B. Kim, M. Chun, and D. Choi, "Microstructures and multiferroic properties of electrospun $BiFeO_3$ nanofibers," *Journal of the Korean Physical Society*, vol. 59, no. 3, pp. 2308–2312, 2011.

[22] N. L. Wei Wang, Y. Chi, Y. J. Li, W. F. Yan, X. T. Li, and C. L. Shao, "Electrospinning of magnetical bismuth ferrite nanofibers with photocatalytic activity," *Ceramics International*, vol. 39, no. 4, pp. 3511–3518, 2013.

[23] P. M. Shaibani, K. Prashanthi, A. Sohrabi, and T. Thundat, "Photocatalytic $BiFeO_3$ nanofibrous mats for effective water treatment," *Journal of Nanotechnology*, vol. 2013, Article ID 939531, 6 pages, 2013.

[24] Y. Wang, Q. Jiang, H. He, and C. Nan, "Multiferroic $BiFeO_3$ thin films prepared via a simple sol-gel method," *Applied Physics Letters*, vol. 88, no. 14, Article ID 142503, 2006.

[25] S. Li, Y. Lin, B. Zhang, Y. Wang, and C. Nan, "Controlled fabrication of $BiFeO_3$ uniform microcrystals and their magnetic and photocatalytic behaviors," *Journal of Physical Chemistry C*, vol. 114, no. 7, pp. 2903–2908, 2010.

[26] Y. Wang and C. Nan, "Site modification in $BiFeO_3$ thin films studied by Raman spectroscopy and piezoelectric force microscopy," *Journal of Applied Physics*, vol. 103, no. 11, Article ID 114104, 2008.

[27] C.-W. Nan and Y. Wang, "Site modification in $BiFeO_3$ thin films studied by Raman spectroscopy and piezoelectric force microscopy," *Journal of Applied Physics*, vol. 103, no. 11, Article ID 114104, 2008.

[28] S. V. Fridrikh, J. H. Yu, M. P. Brenner, and G. C. Rutledge, "Controlling the fiber diameter during electrospinning," *Physical Review Letters*, vol. 90, no. 14, Article ID 144502, pp. 1–4, 2003.

[29] R. Guo, L. Fang, W. Dong, F. Zheng, and M. Shen, "Magnetically separable $BiFeO_3$ nanoparticles with a γ-Fe_2O_3 parasitic phase: controlled fabrication and enhanced visible-light photocatalytic activity," *Journal of Materials Chemistry*, vol. 21, no. 46, pp. 645–652, 2011.

[30] V. I. Klimov, S. A. Ivanov, J. Nanda et al., "Single-exciton optical gain in semiconductor nanocrystals," *Nature*, vol. 447, no. 7143, pp. 441–446, 2007.

[31] W. W.-F. Leung and C. C. Pei, "Enhanced photocatalytic activity of electrospun TiO_2/ZnO nanofibers with optimal anatase/rutile ratio," *Catalysis Communications*, vol. 37, pp. 100–104, 2013.

[32] M. A. Butler, "Photoelectrolysis and physical properties of the semiconducting electrode WO_2," *Journal of Applied Physics*, vol. 48, no. 5, pp. 1914–1920, 1977.

[33] A. J. Hauser, J. Zhang, L. Mier et al., "Characterization of electronic structure and defect states of thin epitaxial $BiFeO_3$ films by UV-visible absorption and cathodoluminescence spectroscopies," *Applied Physics Letters*, vol. 92, no. 22, Article ID 222901, 2008.

[34] K. Takahashi, N. Kida, and M. Tonouchi, "Terahertz radiation by an ultrafast spontaneous polarization modulation of multiferroic $BiFeO_3$ thin films," *Physical Review Letters*, vol. 96, no. 11, Article ID 117402, 2006.

[35] B. B. Kale, J. Baeg, S. M. Lee, H. Chang, S. Moon, and C. W. Lee, "CdIn2S4 nanotubes and "marigold" nanostructures: a visible-light photocatalyst," *Advanced Functional Materials*, vol. 16, no. 10, pp. 1349–1354, 2006.

[36] Q. Liu, Y. Zhou, J. Kou et al., "High-yield synthesis of ultralong and ultrathin Zn_2GeO_4 nanoribbons toward improved photocatalytic reduction of CO_2 into renewable hydrocarbon fuel,"

Journal of the American Chemical Society, vol. 132, no. 41, pp. 14385–14387, 2010.

[37] L. W. Martin, S. P. Crane, Y.-H. Chu et al., "Multiferroics and magnetoelectrics: thin films and nanostructures," *Journal of Physics Condensed Matter*, vol. 20, no. 43, Article ID 434220, 2008.

[38] F. Kubel and H. Schmid, "Structure of a ferroelectric and ferroelastic monodomain crystal of the perovskite $BiFeO_3$," *Acta Crystallographica Section B*, vol. 46, no. 6, pp. 698–702, 1990.

[39] A. V. Zalesskii, A. K. Zvezdin, A. A. Frolov, and A. A. Bush, "57Fe NMR study of a spatially modulated magnetic structure in $BiFeO_3$," *JETP Letters*, vol. 71, no. 11, pp. 465–468, 2000.